Korean J. Chem. Eng., 40(3), 504-511 (2023)
DOI: 10.1007/s11814-022-1260-7

pISSN: 0256-1115
eISSN: 1975-7220

Dual-effect-assisted cross-linkable poly(N-allyl-vinylimidazolium)·$TFSI^-$ as alternative electrode binder of lithium-ion battery

Hui Gyeong Park*,‡, Yoon Kook Son,‡, Jiseong Kim***, and Jung-Soo Lee*,***,†**

*Department of Chemical Engineering, Graduate School, Chosun University, 309 Pilmun-daero, Dong-gu, Gwangju 61452, Korea
**Department of Electrical Engineering, Chosun University, 309 Pilmun-daero, Dong-gu, Gwangju 61452, Korea
***Department of Bio-Chemical Engineering, Chosun University, 309 Pilmun-daero, Dong-gu, Gwangju 61452, Korea
(*Received 12 July 2022 • Revised 9 August 2022 • Accepted 17 August 2022*)

Abstract−The increasing demand for electric vehicles, portable electronic devices, and energy storage devices has spurred interest in the development of high-capacity rechargeable lithium-ion batteries (LIBs). Polyionic liquids are used in LIB binders or electrolytes owing to their favorable physical properties. Chemical cross-linking of polymer binders has been proposed as an effective and simple method for increasing the volume of electrodes. The designed polymer binder offers high ion conductivity and robustness via an appropriate adjustment of the solid electrolyte interphase layer and chemical cross-linking during the electrochemical test. A cross-linked poly(N-allyl-vinyl imidazolium) (C-PAVIm)-based electrode can improve the cycle properties by decreasing the overpotential and allowing Li^+ to flow at the interface between the active material and electrolyte. The surface of a C-PAVIm-based electrode is monitored via scanning electron microscopy and X-ray photoelectron spectroscopy. Electrochemical impedance spectroscopy results show that the C-PAVIm-based electrode after cycling exhibits a thinner solid electrolyte interphase layer and a lower diffusion resistance as compared with a poly(vinylidene fluoride) (PVDF)-based electrode. Therefore, the C-PAVIm-based electrode exhibits better charge-discharge stability than the PVDF-based electrode. These findings imply that polymer binders with appropriately designed chemical structures can improve the electrochemical performance of LIB systems.

Keywords: Lithium-ion Batteries, Polyionic Liquid, Binder, Cross-linking, Solid Electrolyte Interphase Layer

INTRODUCTION

The increasing demand for electric vehicles, portable devices, and grid-scale energy storage devices has spurred interest in the development of high-capacity rechargeable lithium-ion batteries (LIBs) [1,2]. However, the cost, performance, and energy density of LIBs have not been improved adequately for the development of stable, high-capacity electrode materials [3]. To satisfy the abovementioned demands, researchers have extensively investigated materials for electrodes, such as active materials, conductive agents, and polymer binders, in the past few decades. Active materials for improving the cycling stability and capacity of LIBs have been prioritized, whereas polymer binders are rarely investigated [4-8]. Polymer binders, as an integral component of LIBs, are vital to cycling stability as they provide interconnectivity and adhesive ability among the electrodes of LIBs [9]. In addition, the initial capacity loss and formation of a harmful solid electrolyte interphase (SEI), which occurs due to the interaction of the polymer binder at the interface between the electrode and electrolyte, have not been investigated sufficiently [10-15]. Furthermore, as new active materials for next-generation LIBs are being extensively investigated, the appropriate chemical structure of the polymer binder must be determined concurrently.

Polymer binders should maintain stable adhesion characteristics without side reactions, including in electrochemical environments; in this regard, poly(vinylidene fluoride) (PVDF) is typically used as a representative polymer binder [16-18]. PVDF is currently the standard for lithium battery technology and is used commercially in LIBs owing to its favorable adhesion, chemical inertness, and process availability [19,20]. However, the most significant disadvantage of PVDF binders is their insulating property and considerable electrolyte swelling [6,21]. Hence, a passivation layer known as an SEI layer is typically formed on the surface of the electrodes to create a barrier from the decomposition products of the electrolyte. However, the formation and growth of the SEI layer results in decreased capacity, increased battery resistance, and reduced power density. Hence, a new binder design is required [1,22].

Polyionic liquids (PILs), which have recently garnered attention for their excellent electrochemical stability, ion conductivity, and processability, are sustainable for electrochemical applications [23-27]. PILs are not only a promising class of functional polymers, but are also highly stable for use as LIB materials [28]. PILs can suppress the formation of an SEI and improve cycle properties by decreasing the overpotential and allowing Li^+ to flow at the interface between the active material and electrolyte [29,30].

Chemical cross-linking of polymer binders has been proposed as an effective and simple method for the volume expansion of electrodes [31]. Moreover, the cross-linked polymer binder can improve the binding force of each component of the electrode and minimize the effects of swelling during the charging and discharging of

†To whom correspondence should be addressed.
E-mail: jslee15@chosun.ac.kr
‡These authors contributed equally to this study.

the electrode [32-34].

In summary, the design of the interface between the electrode and electrolyte is crucial in improving the function and performance of LIBs. Systematic designs of functional polymer binders that affect the electrode interface will promote battery research. Herein, we introduce an unconventional binder, i.e., a high-performance binder that is cross-linkable and ion conductive during direct fabrication. This polymer binder offers high ion conductivity and robustness by the appropriate adjustment of the SEI layer and chemical cross-linking. Furthermore, it is expected to prevent a further reduction of the electrolytes. We demonstrate that the polymer binder results in the excellent performance and high stability of LIBs, and explain the mechanical process for supporting electrochemical reactions. In summary, this paper focuses on the development of multifunctional binders that can form a highly ion-conductive SEI and improve the cycle life and performance of LIBs, thereby outperforming currently used commercial binders.

EXPERIMENTAL

1. Materials

In this study, 1-vinyl imidazole (Vm) (Alfa Aesar), a,a′-azobisisobutyronitrile (AIBN) (JUNSEI), dimethylformamide (DMF) (JUNSEI), acetone (Duksan, extra pure grade), allyl bromide (Sigma-Aldrich), methanol (MeOH) (REAGENTS DUKSAN), diethyl-ether (Duksan extra pure grade), lithium bis(trifluoromethanesulfonyl)imide (LiTFSI) (Duksan) were used without any further purification. AIBN was recrystallized from MeOH.

2. Synthesis of Poly(vinyl Imidazole) (PVIm)

Vm (monomer, 4 g), AIBN (initiator, 0.04 g), and DMF (15 mL) were mixed together in a flask. Subsequently, the flask was degassed and filled with nitrogen, a process repeated several times. Next, the mixture was reacted at 70 °C for 24 h via magnetic stirring. After natural cooling, the mixture was precipitated using acetone (300 mL). The powdered product was filtered and dissolved in acetone several times. The product was then dried overnight under dry vacuum at 60 °C.

3. Quaternization of PVIm with Allyl Bromide

PVIm (2 g), allyl bromide (3.0789 g), and MeOH (65 mL) were added to a round-bottom flask and allowed to react at 40 °C for 48 h under magnetic stirring. After the reaction was terminated, the mixed solution was precipitated with diethyl ether (1 L). Finally, the product was dried overnight in a vacuum oven at 40 °C, as shown in Scheme 1.

4. Anion Exchange of Poly(N-allyl-vinyl Imidazolium)·$TFSI^-$ (PAVIm·$TFSI^-$)

An ion exchange reaction was performed to obtain PAVIm·Br^- and TFSI by solubilizing PAVIm·Br^- (1 g) in deionized water, followed by the dropwise addition of an aqueous solution of LiTFSI (2 g). The mixture was then stirred at room temperature for 10 h. Next, the precipitated powder was washed with deionized water in an aspirator and dried overnight in a vacuum oven at 40 °C.

5. Thermal Cross-linked Poly(N-allyl-vinyl Imidazolium)·$TFSI^-$ (C-PAVIm·$TFSI^-$)

The prepared PAVIm·$TFSI^-$ films were placed in a vacuum oven at 100 °C for 1 h (C-PAVIm 0), 150 °C for 1 h (C-PAVIm 1) and 2 h (C-PAVIm 2), and 160 °C for 1 h (C-PAVIm 3) to cross-link them thermally.

6. Characterization

The chemical structure of the films was analyzed via Fourier-transform infrared spectrometry (FT-IR, Nicolet6700) and proton nuclear magnetic resonance (^{1}H-NMR, JEOL-JNM-AL300) in DMSO-d_6 at 300 MHz. The thermal property of C-PAVIm was investigated using differential scanning calorimetry (DSC, TA Instruments DSC25) under an N_2 atmosphere (at a temperature range of 25 °C-180 °C and a heating rate of 5 °C min^{-1}) and via thermogravimetric analysis (TGA, TA Instruments SDT650) under an N_2 atmosphere (at a temperature range of 25 °C-1,000 °C and a heating rate of 10 °C min^{-1}). To confirm the degree of chemical cross-linking, the gel content was determined using the solvent extraction method and calculated using the following equation:

$$\frac{M_2}{M_1} \times 100\% = \text{gel content},$$

where M_1 is the weight of C-PAVIm and M_2 is the weight of the extracted solvent [35].

Morphological and chemical characterization of the electrode was by scanning electron microscopy (SEM, Hitachi Regulus 8100) and X-ray photoelectron spectroscopy (XPS, Thermo Scientific, NEXSA) before and after the electrochemical cycle test.

7. Electrochemical Characterization

All electrodes, including the cross-linked binder (C-PAVIm) and PVDF (1100, Kureha Chemical Industry, Japan, 10 wt%), were manufactured based on the same composition ratio. The constituent materials were a Si-graphite composite as the active material, C-PAVIm and PVDF as the binder and Super-P (Timcal Inc.) as the conductive material, in a mass ratio of 88 : 8 : 4. A binder solution comprising C-PAVIm and PVDF was adopted, along with 4 wt% of NMP solvent. The loading levels of all manufactured electrodes were approximately 3 mg cm^{-2}. We utilized 1.15 M $LiPF_6$ in ethylene carbonate (EC)/ethyl methyl carbonate/dimethyl carbonate (DEC) (at a ratio of 3 : 5 : 2 (v/v)) and microporous polyethylene as the electrolyte and separator, respectively. A 2032R coin cell assembled in an argon-filled glove box was used for all electrochemical tests. It was tested for charging/discharging at 0.05C (1C=550 mA g^{-1}) for the formation cycle, 1.0C for the cycle life test and 0.2C, 0.5C, 1.0C, 3.0C and 5.0C for rate capability tests in the voltage range of 1.5 to 0 V at 26 Â °C. Charging was performed at a constant current mode. Electrochemical impedance spectroscopy (EIS, IVIUM) was conducted to confirm the impedance at a frequency range of 0.003-300 kHz and an amplitude of 1.5 V for the pristine samples and samples that underwent 20 charging cycles at 26 °C.

RESULT AND DISCUSSION

Free radical polymerization, one of the most typical and favored techniques used in chemistry, converts low-molecular-weight monomers into polymers by the successive addition of free radicals in the presence of an initiator. The quaternization of amines is an extensively investigated reaction in the chemistry of ionic liquids. Quaternization maximizes the distance between the substituents on an annular N via an S_N2 mechanism. It is the most effective method

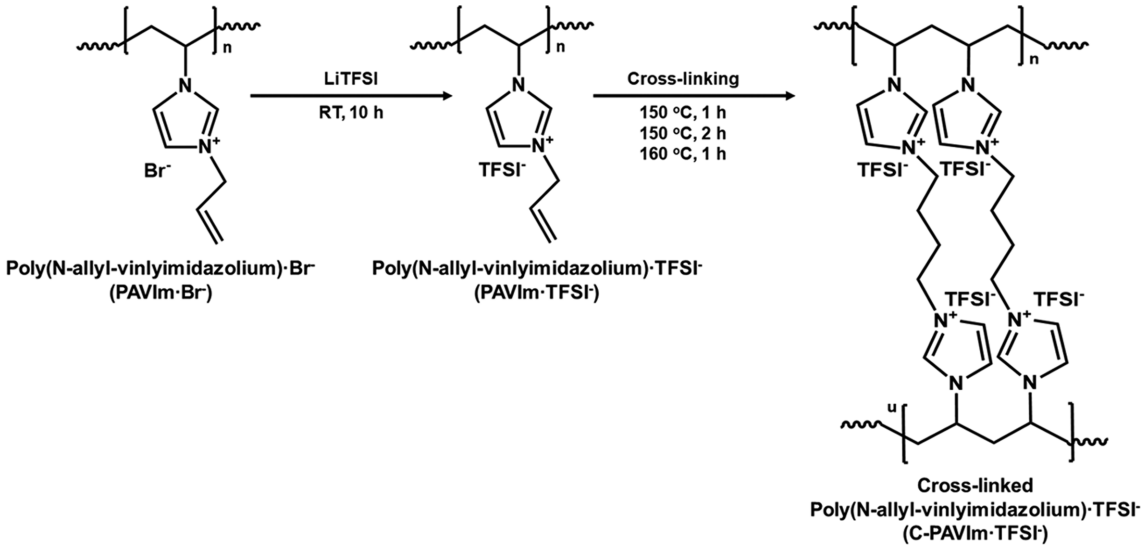

Fig. 1. Schematic illustration showing synthesis of C-PAVIm.

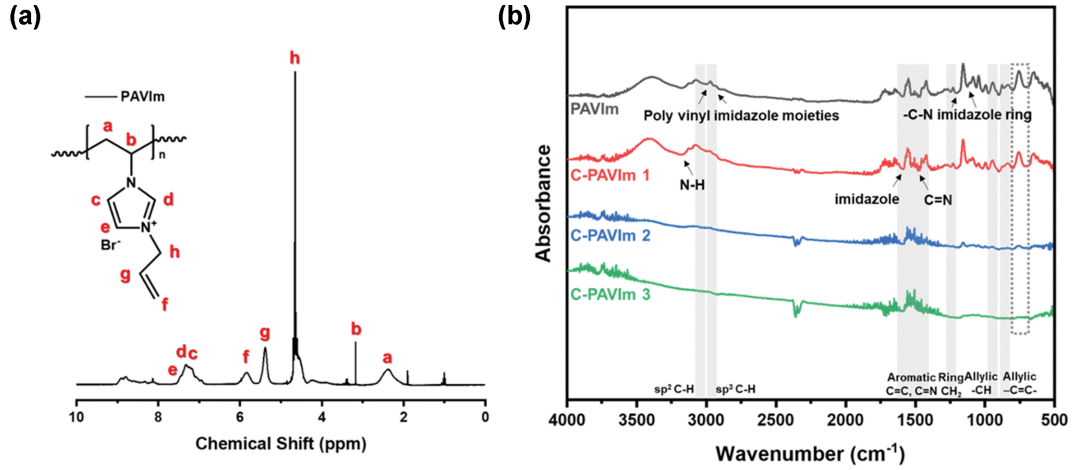

Fig. 2. (a) ^{1}H-NMR spectra of PAVIm; (b) FT-IR spectra of PAVIm and C-PAVIm.

for functionalizing positions adjacent to a nitrogen atom to enhance ion conductivity. In this study, we successfully synthesized PVIm via the free radical polymerization of Vm using AIBN as the initiator (Fig. S1). We quarternized PVIm with allyl bromide as the functional group via an aromatic S_N2 reaction under mild conditions. Consequently, PAVIm with both ionic conductivity and cross-linkable groups was obtained. Br^- ions were exchanged with $TFSI^-$ ions via an anion exchange reaction to be applied to LIBs, as shown in Fig. 1.

In the ^{1}H-NMR analysis, the signals at 1.6-2.2 ppm (H_a) 2.8-3.2 ppm (H_b) were ascribed to the backbone protons (CH_2 and CH-, respectively). This suggests the successful polymerization of the vinyl group of 1-Vinylimidazole, as shown in Fig. S2(a). The proton resonance in the imidazole ring (H_c, H_d and H_e) shifted to 7.0-8.0 ppm, owing to the allyl(vinyl) group at 5-6.2 ppm (H_f, H_g and H_h), as shown in Fig. 2(a). Thus, the well-defined peaks signify that the synthesis and quaternization had proceeded [36-38].

The chemical structure of PAVIm and C-PAVIm was confirmed using FT-IR spectroscopy (Fig. 2(b)). The ordinary peaks at 3,100-3,000 cm^{-1} and 2,950-2,800 cm^{-1} are attributable to sp^2 C-H and sp^3 C-H, respectively. The peaks at 2,916 and 2,846 cm^{-1} are attributed to the polyvinyl imidazole moieties [39]. The characteristic peaks at 1,170 and 1,126 cm^{-1} are attributed to the C-N asymmetric stretching frequency of the imidazole ring, whereas the peaks at 1,750-1,550 cm^{-1} are attributed to the -C=N stretching of the imidazole ring [40]. The emergence of the two peaks at 992 and 944 cm^{-1} is due to the allylic moieties. In particular, the alkane of the allyl group decreased at peaks of 730-720 cm^{-1} (dotted gray square) as the temperature increased for thermal cross-linking. In addition, the peak at 1,335-1,250 cm^{-1} decreased due to the degradation of aromatic amines in C-PAVIm 2 and C-PAVIm 3 [38,41, 42]. Thus, C-PAVIm 1 was considered the optimal condition.

Methods to improve the physical properties of polymers include blending, composite utilization and cross-linking. Cross-linking between polymer chains is a simple yet effective method. The typical method of cross-linking between double bonds involves the

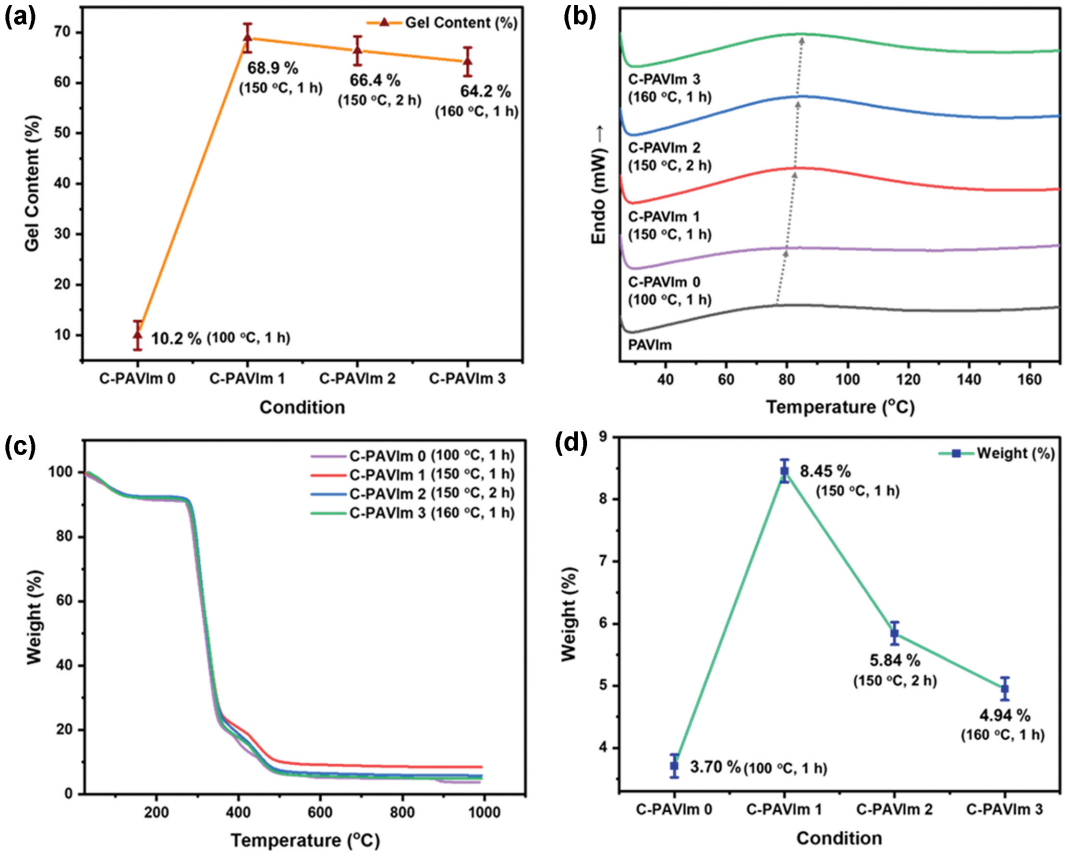

Fig. 3. (a) Gel content of C-PAVIm 0, C-PAVIm 1, C-PAVIm 2, and C-PAVIm 3; (b) DSC thermograms; (c) TGA thermograms; (d) final weight based on TGA.

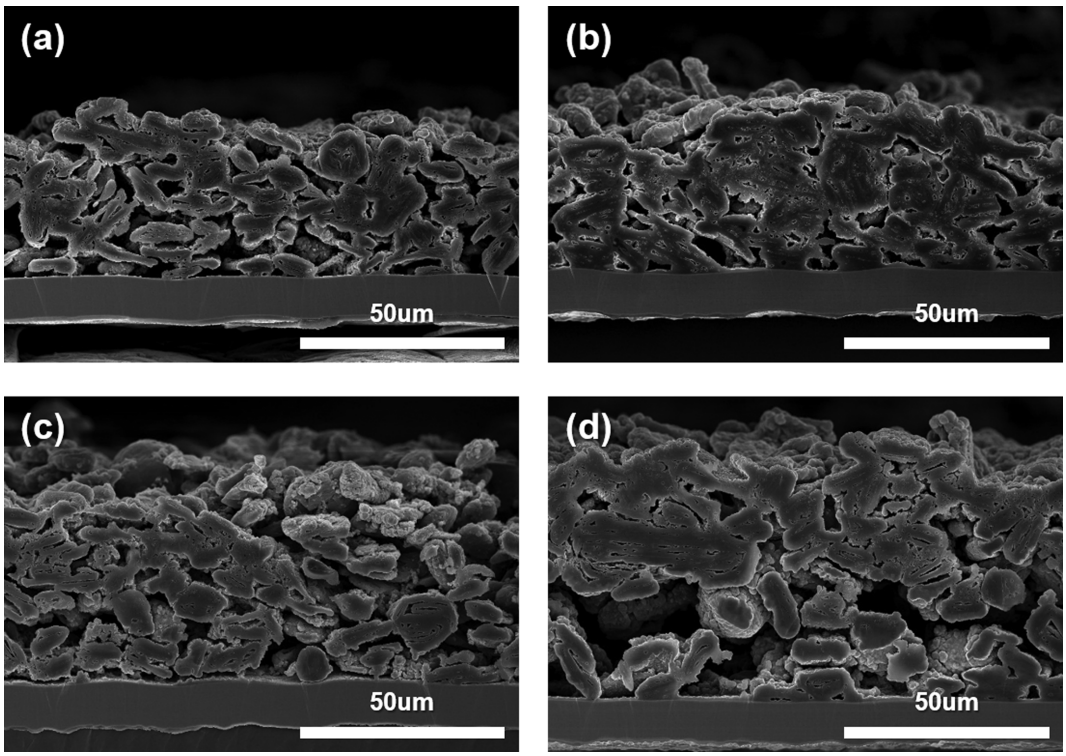

Fig. 4. SEM images showing cross-section of electrode: PVDF (a) before and (b) after 20 cycles; C-PAVIm 1 (c) before and (d) after 20 cycles at 1.0C.

direct utilization of an initiator or the delivery of energy. However, initiators are difficult to remove after cross-linking and additives may introduce side reactions during battery testing [43]. Thus, energy is transferred to conduct cross-linking via the most accessible heat treatment. To confirm the cross-linking degree, the gel content of C-PAVIm was measured at different temperatures during thermal treatment, as shown in Fig. 3(a). The gel content increased with the thermal treatment temperature until 150 °C (C-PAVIm 1), above which it saturated. At conditions higher than C-PAVIm 1, the gel content decreased slightly owing to the collapse of the polymeric chemical structure, as confirmed via FT-IR analysis.

The thermal property of the C-PAVIm prepared via thermal treatment was analyzed using DSC and TGA; the results are shown in Figs. 3(b) and (c). DSC analysis was performed to confirm the thermal characteristics of the prepared C-PAVIm. The data show that the glass transition temperature of the prepared samples increased with the cross-linking temperature. The TGA results indicate that the final weight of C-PAVIm 1 was the highest (Fig. 3(d)). Therefore, these results confirm that the thermal properties of C-PAVIm enhanced under controlled conditions.

Electrochemical tests were conducted using a selected condition, where C-PAVIm 1 was used as the anode binder of the LIBs. The cross-sectional morphological status of the anode electrodes was observed after 20 charge/discharge cycles via SEM and the results are shown in Fig. 4 [44].

The PVDF-based electrode exhibited clear swelling and a thick SEI layer, as shown in Fig. 4(b). By contrast, the C-PAVIm-based electrode exhibited less swelling and a thinner SEI layer, as shown in Fig. 4(d). Thus, the SEM images confirmed that the C-PAVIm binder participated in the formation of the SEI layer owing to the degradation of the electrolyte and contributed positively to the cycling performance.

To further understand the chemical composition of the formed SEI, XPS analysis was performed on the silicon anode electrodes before and after 20 cycles, and the results are shown in Figs. 5(a) and (b). The peak at approximately 289 eV was assigned to Li_2CO_3 and RO-COO. Li_2CO_3 and RO-COO have been widely reported as the main components of SEIs formed on silicon. Based on the electrochemical reaction, the most likely principal component is Li_2CO_3, owing to the decomposition of the DMC electrolyte [45]. The relative intensities of the Li_2CO_3 and RO-COO peaks in the PVDF-based electrodes after 20 cycles were much higher than those of the C-PAVIm-based electrode. In addition, C=O and C-OH bonds were formed at 287 and 286 eV, respectively [46-51]. Therefore, the stable cycling performance and SEI formation are attributable to the C-PAVIm of the cross-linked network and ionic

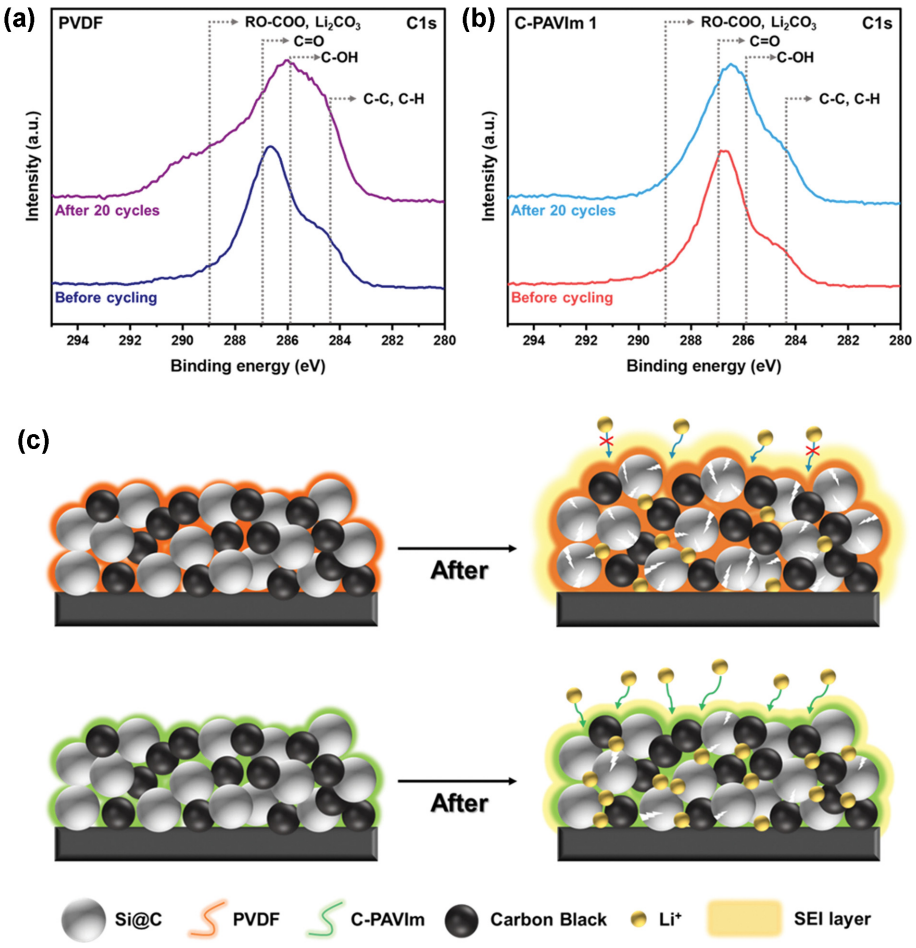

Fig. 5. XPS spectra for before cycling and after 20 cycles: (a) PVDF C1s; (b) C-PAVIm 1 C1s. (c) Li electron conduction of PVDF and C-PAVIm in Si electrodes.

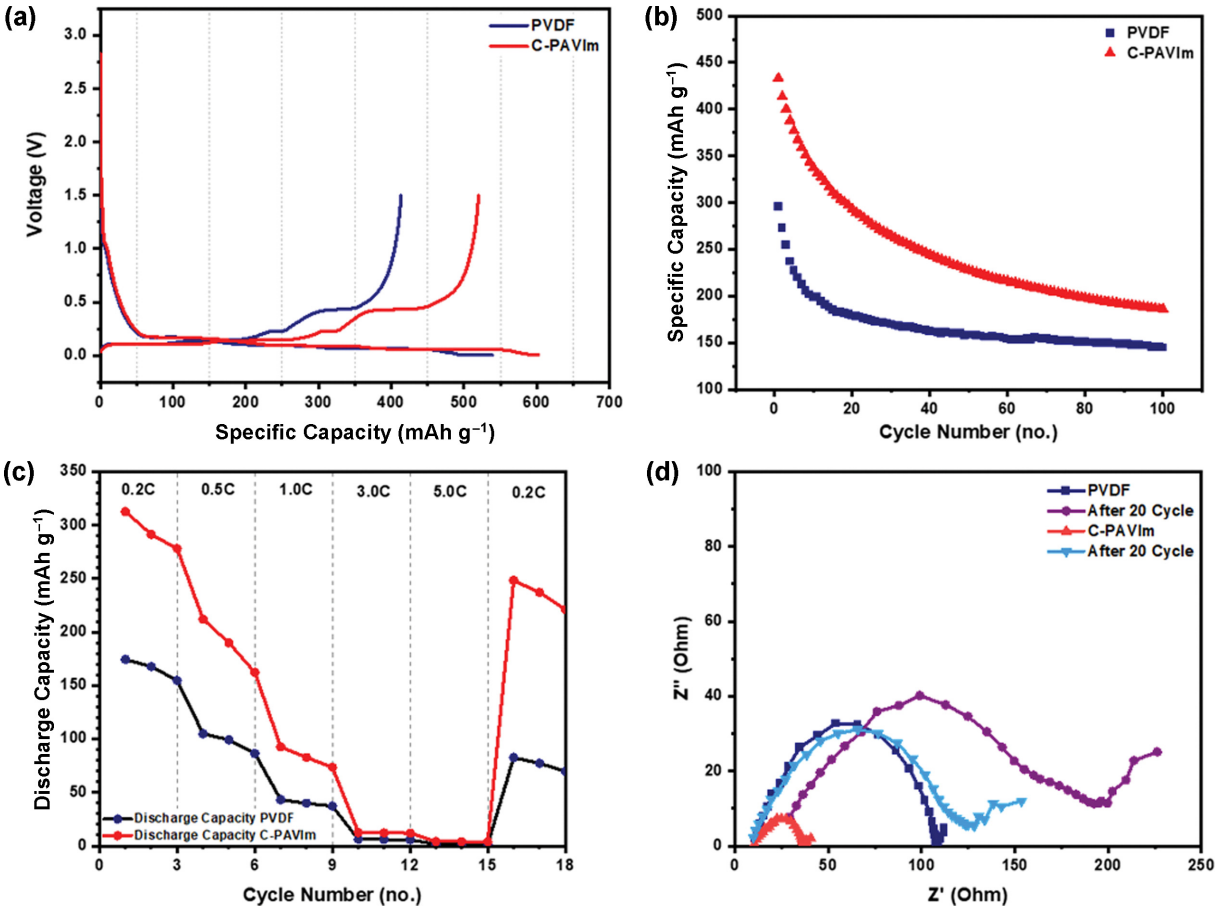

Fig. 6. (a) Charge-discharge profiles during first cycle for Si-graphite composite anodes with C-PAVIm as a binder; (b) cycling performance of Si-graphite composite anodes with C-PAVIm (red) and PVDF as binders and 1.0 M $LiPF_6$/EC : DEC electrolyte at 1C; (c) rate capability performance of Si-graphite composite anodes with C-PAVIm (red) and PVDF (black) as binders and 1.0 M $LiPF_6$/EC:DEC electrolyte; (d) electrochemical impedance spectra (EIS) profiles at 26 °C for charging cycles of PVDF after formation, PVDF 20 cycles, C-PAVIm after formation and C-PAVIm after 20 cycles.

conductivity on the surface of the silicon nanoparticles.

The enhanced performance in the presence of silicon nanoparticles and C-PAVIm 1 can be explained based on the schematic illustration shown in Fig. 5(c). Our designed C-PAVIm shows that the ionic conductivity and robustness of the electrode improved owing to the formation of an appropriate SEI layer and thermal cross-linking. Meanwhile, PVDF formed a thick SEI layer, which inhibited ion conductivity and disintegrated the structure of the silicon nanoparticles. Hence, we focused on multifunctional binder designs that can enhance lithium-ion transport by supporting the formation of a conductive SEI, thereby affording a longer cycle life and improved overall LIB performance.

Fig. 6(a) shows the charge-discharge profile of the first cycle at 0.05C for the electrodes composed of C-PAVIm and PVDF, separately. In the first cycle, an irreversible reaction was observed at approximately 0.7 V, which resulted in the formation of an SEI. The C-PAVIm electrode demonstrated superior discharge and charge capacity of 610 and 520 mAh g^{-1}, respectively, as compared with the PVDF electrode. This implies that the C-PAVIm electrode can offer a better Li pathway and a lower ionic resistance [30]. The C-PAVIm electrode exhibited a higher discharge capacity than the PVDF electrode during the cycling life test (Fig. 6(b)). After 100 cycles, the C-PAVIm and PVDF electrodes indicated saturated capacity of 190 and 105 mAh g^{-1}, respectively. This implies that the C-PAVIm electrode offers a more efficient transfer of Li even after long charge/discharge cycles. Additionally, the characteristics above were reflected in the rate capability result. The rate capability of the electrodes composed of C-PAVIm and PVDF was verified up to 5.0C. Based on the rate capability, we believe that the low Li ion diffusivity of the PVDF electrode resulted in inferior electrical power properties, as compared with the C-PAVIm electrode. To further investigate the superior performance of C-PAVIm electrode, EIS was conducted on the electrodes composed of C-PAVIm and PVDF after the formation and 20th cycles, respectively. The diameter of the semicircle in the higher frequency region was ascribed to the charge transfer resistance (R_{ct}), which is associated with the chemical reaction between the electrolyte and active material interface. After the formation cycle, the PVDF electrode indicated a higher value of R_{ct}, which would result in a higher Li ion transfer rate. After the 20th cycle, the R_{ct} of the PVDF electrode increased more significantly than that of the C-PAVIm electrode. Additionally, it remained larger than that of the C-PAVIm electrode, which implies that the PVDF

electrode possessed a more unstable interface with the electrolyte as compared with the C-PAVIm electrode. These EIS results are consistent with the other electrochemical results presented above. Furthermore, the solution resistance of the PVDF electrode increased significantly after the 20th cycle, whereas that of the C-PAVIm electrode remained the same. This implies that the PVDF electrode exhausted the electrolyte continuously during the cycling test owing to the unstable interface between the active materials and electrolyte.

CONCLUSION

We have demonstrated that a cross-linked binder comprising cyclic polymers can be utilized to improve cycling performance. C-PAVIm, as a binder in Si anodes, performed better than the commercially employed PVDF binder. Anodes based on the C-PAVIm binder formed a better SEI than those based on the PVDF binder. Consequently, the charge-discharge performance of the C-PAVIm binder was improved. In addition, the C-PAVIm binder indicated better rate performance and a higher discharge capacity than the PVDF binder at high charge-discharge rates, thus indicating its high stability. Consequently, the interaction of the C-PAVIm binder with the electrode material improved and the current collector enabled the integrity of the electrode to be maintained over a long cycling period. These results indicate that C-PAVIm is a potential alternative to PVDF as a binder in LIBs. These innovative binders will provide a practical solution for polymeric binders, which are highly promising electrode materials. In the future, PAVIm binders might prove to be effective.

ACKNOWLEDGEMENTS

This study was supported by a National Research Foundation of Korea (NRF) grant funded by the Korean government (MSIT; Ministry of Science and ICT) (Nos. 2020R1I1A3071687 and 2020 R1A4A1019463).

SUPPORTING INFORMATION

Additional information as noted in the text. This information is available via the Internet at http://www.springer.com/chemistry/journal/11814.

REFERENCES

1. M. Wu, X. Xiao, N. Vukmirovic, S. Xun, P. K. Das, X. Song, P. Olalde-Velasco, D. Wang, A. Z. Weber, L.-W. Wang, V. S. Battaglia, W. Yang and G. Liu, *J. Am. Chem. Soc.*, **135**, 12048 (2013).
2. M. M. Thackeray, C. Wolverton and E. D. Isaacs, *Energy Environ. Sci.*, **5**, 7854 (2012).
3. M. Armand and J. M. Tarascon, *Nature*, **451**, 652 (2008).
4. A. Cholewinski, P. Si, M. Uceda, M. Pope and B. Zhao, *Polymers*, **13**, 631 (2021).
5. J. Liu, Q. Zhang and Y.-K. Sun, *J. Power Sources*, **396**, 19 (2018).
6. H. Chen, M. Ling, L. Hencz, H. Y. Ling, G. Li, Z. Lin, G. Liu and S. Zhang, *Chem. Rev.*, **118**, 8936 (2018).
7. A. Miranda, K. Sarang, B. Gendensuren, E.-S. Oh, J. Lutkenhaus and R. Verduzco, *Mol. Syst. Des. Eng.*, **5**, 709 (2020).
8. Y. Shi, X. Zhou and G. Yu, *Acc. Chem. Res.*, **50**, 2642 (2017).
9. D. Bresser, D. Buchholz, A. Moretti, A. Varzi and S. Passerini, *Energy Environ. Sci.*, **11**, 3096 (2018).
10. S. K. Heiskanen, J. Kim and B. L. Lucht, *Joule*, **3**, 2322 (2019).
11. R. Fong, U. von Sacken and J. R. Dahn, *J. Electrochem. Soc.*, **137**, 2009 (1990).
12. P. Verma, P. Maire and P. Novák, *Electrochim. Acta*, **55**, 6332 (2010).
13. K. H. Kim, J. H. Cho, J. U. Hwang, J. S. Im and Y.-S. Lee, *J. Ind. Eng. Chem.*, **99**, 48 (2021).
14. S. Chen, J. Zheng, L. Yu, X. Ren, M. H. Engelhard, C. Niu, H. Lee, W. Xu, J. Xiao, J. Liu and J.-G. Zhang, *Joule*, **2**, 1548 (2018).
15. Z. Hu, S. Zhang, S. Dong, W. Li, H. Li, G. Cui and L. Chen, *Chem. Mater.*, **29**, 4682 (2017).
16. H. Zheng, R. Yang, G. Liu, X. Song and V. S. Battaglia, *J. Phys. Chem. C*, **116**, 4875 (2012).
17. P. Periasamy, K. Tatsumi, M. Shikano, T. Fujieda, Y. Saito, T. Sakai, M. Mizuhata, A. Kajinami and S. Deki, *J. Power Sources*, **88**, 269 (2000).
18. A. Magistris, P. Mustarelli, F. Parazzoli, E. Quartarone, P. Piaggio and A. Bottino, *J. Power Sources*, **97-98**, 657 (2001).
19. J. Chen, J. Liu, Y. Qi, T. Sun and X. Li, *J. Electrochem. Soc.*, **160**, A1502 (2013).
20. M. M. Loghavi, S. Bahadorikhalili, N. Lari, M. H. Moghim, M. Babaiee and R. Eqra, *Z. Phys. Chem. (N F)*, **234**, 381 (2020).
21. V. A. Nguyen and C. Kuss, *J. Electrochem. Soc.*, **167**, 065501 (2020).
22. J. Zhao, X. Yang, Y. Yao, Y. Gao, Y. Sui, B. Zou, H. Ehrenberg, G. Chen and F. Du, *Adv. Sci.*, **5**, 1700768 (2018).
23. J. Yuan, D. Mecerreyes and M. Antonietti, *Prog. Polym. Sci.*, **38**, 1009 (2013).
24. J. Yuan and M. Antonietti, *Polymer*, **52**, 1469 (2011).
25. W. Qian, J. Texter and F. Yan, *Chem. Soc. Rev.*, **46**, 1124 (2017).
26. G. Gebresilassie Eshetu, M. Armand, B. Scrosati and S. Passerini, *Angew. Chem. Int. Ed.*, **53**, 13342 (2014).
27. M. Armand, F. Endres, D. R. MacFarlane, H. Ohno and B. Scrosati, *Nat. Mater.*, **8**, 621 (2009).
28. I. Spanos, S. Neugebauer, R. Guterman, J. Yuan, R. Schlögl and M. Antonietti, *Sustain. Energy Fuels*, **2**, 1446 (2018).
29. T. P. Jayakumar, R. Badam and N. Matsumi, *ACS Appl. Energy Mater.*, **3**, 3337 (2020).
30. J.-S. Lee, K. Sakaushi, M. Antonietti and J. Yuan, *RSC Adv.*, **5**, 85517 (2015).
31. L. E. Nielsen, *J. Macromol. Sci. A*, **3**, 69 (1969).
32. J. Lopez, Z. Chen, C. Wang, S. C. Andrews, Y. Cui and Z. Bao, *ACS Appl. Mater. Interfaces*, **8**, 2318 (2016).
33. R. Rohan, T.-C. Kuo, C.-Y. Chiou, Y.-L. Chang, C.-C. Li and J.-T. Lee, *J. Power Sources*, **396**, 459 (2018).
34. J. Yuan, S. Prescher, K. Sakaushi and M. Antonietti, *J. Mater. Chem.*, **3**, 7229 (2015).
35. J.-S. Lee, C.-H. Jung, S.-Y. Jo, J.-H. Choi, I.-T. Hwang, Y.-C. Nho, Y.-M. Lee and J.-S. Lee, *J. Polym. Sci. A Polym.*, **48**, 2725 (2010).
36. X. L. Huang, C. X. Lin, E. N. Hu, F. Soyekwo, Q. G. Zhang, A. M. Zhu and Q. L. Liu, *RSC Adv.*, **7**, 27342 (2017).
37. C. Zhou, H. Song, F. Zhang, J. Liu, J. Li, B. Liu and J. Liang, *Polym. Bull.*, **76**, 5433 (2019).
38. D. Guo, Y. Z. Zhuo, A. N. Lai, Q. G. Zhang, A. M. Zhu and Q. L.

Liu, *J. Membr. Sci.*, **518**, 295 (2016).
39. H. El-Hamshary, M. M. G. Fouda, M. Moydeen, M. H. El-Newehy, S. S. Al-Deyab and A. Abdel-Megeed, *Int. J. Biol. Macromol.*, **72**, 1466 (2015).
40. Z. Sekhavat Pour and M. Ghaemy, *RSC Adv.*, **5**, 64106 (2015).
41. A. Sengupta, S. Kumar Ethirajan, M. Kamaz, M. Jebur and R. Wickramasinghe, *Sep. Purif. Technol.*, **212**, 307 (2019).
42. T. Feng, B. Lin, S. Zhang, N. Yuan, F. Chu, M. A. Hickner, C. Wang, L. Zhu and J. Ding, *J. Membr. Sci.*, **508**, 7 (2016).
43. X. Wu, K. Song, X. Zhang, N. Hu, L. Li, W. Li, L. Zhang and H. Zhang, *Front. Energy Res.*, **7** (2019).
44. N. Shimoi, M. Komatsu and Y. Tanaka, *Coatings*, **9**, 732 (2019).
45. Z.-Y. Wu, Y.-Q. Lu, J.-T. Li, S. Zanna, A. Seyeux, L. Huang, S.-G. Sun, P. Marcus and J. Światowska, *ACS Omega*, **6**, 27335 (2021).
46. J.-i. Yamaki, S.-i. Tobishima, K. Hayashi, S. Keiichi, Y. Nemoto and M. Arakawa, *J. Power Sources*, **74**, 219 (1998).
47. Z.-i. Takehara, *J. Power Sources*, **68**, 82 (1997).
48. D. Luo, L. Zheng, Z. Zhang, M. Li, Z. Chen, R. Cui, Y. Shen, G. Li, R. Feng, S. Zhang, G. Jiang, L. Chen, A. Yu and X. Wang, *Nat. Commun.*, **12**, 186 (2021).
49. F. Ding, W. Xu, X. Chen, J. Zhang, M. H. Engelhard, Y. Zhang, B. R. Johnson, J. V. Crum, T. A. Blake, X. Liu and J.-G. Zhang, *J. Electrochem. Soc.*, **160**, A1894 (2013).
50. K. N. Wood and G. Teeter, *ACS Appl. Energy Mater.*, **1**, 4493 (2018).
51. K. T. Sarang, X. Li, A. Miranda, T. Terlier, E.-S. Oh, R. Verduzco and J. L. Lutkenhaus, *ACS Appl. Energy Mater.*, **3**, 6985 (2020).

Supporting Information

Dual-effect-assisted cross-linkable poly(N-allyl-vinylimidazolium)·TFSI⁻ as alternative electrode binder of lithium-ion battery

Hui Gyeong Park*,‡, Yoon Kook Son,‡, Jiseong Kim***, and Jung-Soo Lee*,***,†**

*Department of Chemical Engineering, Graduate School, Chosun University, 309 Pilmun-daero, Dong-gu, Gwangju 61452, Korea
**Department of Electrical Engineering, Chosun University, 309 Pilmun-daero, Dong-gu, Gwangju 61452, Korea
***Department of Bio-Chemical Engineering, Chosun University, 309 Pilmun-daero, Dong-gu, Gwangju 61452, Korea
(*Received 12 July 2022 • Revised 9 August 2022 • Accepted 17 August 2022*)

The cross-linked polymeric binder is prepared by a quaternization of PVIm and allyl bromide (Fig. S1).

Fig. S2(a), the signals at 1.6-2.2 ppm (H_a) 2.8-3.2 ppm (H_b) are ascribed to the backbone protons (CH_2 and CH-). This suggests the successful polymerization of vinyl group of 1-Vinyl imidazole. Likewise, the peaks at around 6.4-7.2 ppm are associated with the protons (H_c, H_d and H_e) on the imidazole ring. The well-defined peaks indicate that the polymerization proceeds smoothly. The NMR spectrum of allyl bromide shows specific peaks at 5-6.2 ppm (H_a, H_b) can be assigned to the protons on the allyl(vinyl) group of the allyl bromide (Fig. S2(b)).

XPS was performed on the silicon electrodes before cycling, after 20 cycles as shown in Fig. S3. C=O, O=C-O were shown. This is believed to be due to oxidation occurring in the manufacturing and storage process of PVDF, C-PAVIm 1 binder.

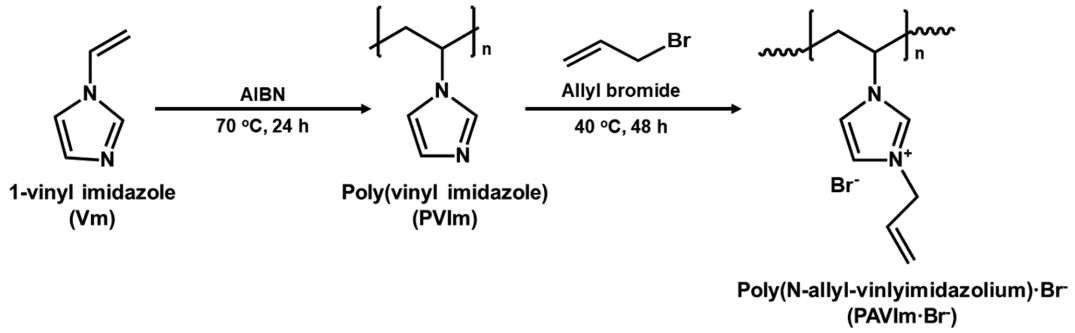

Fig. S1. Schematic illustration showing synthesis of PAVIm.

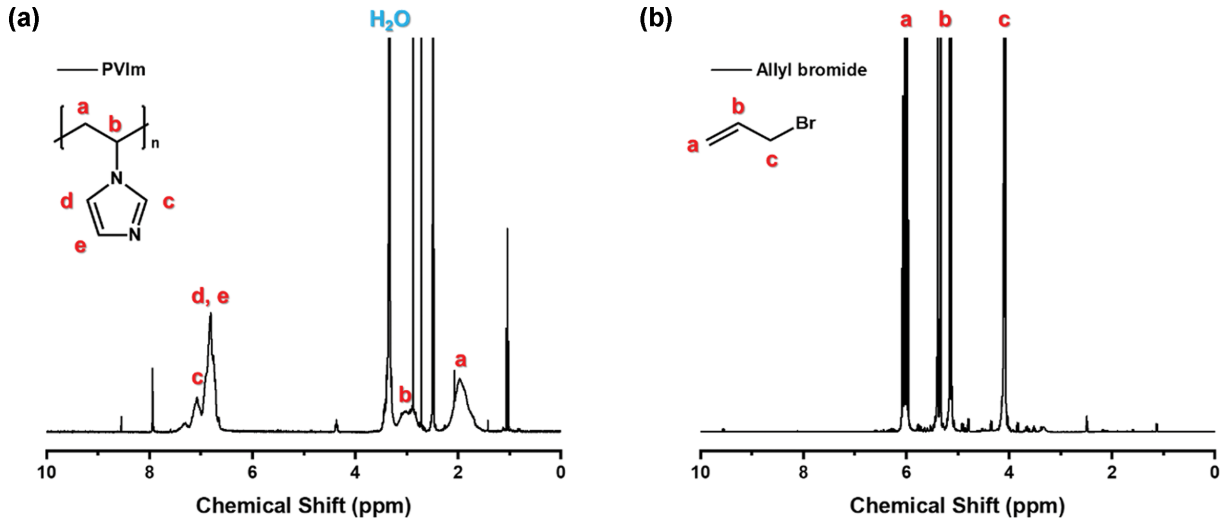

Fig. S2. (a) ^{1}H-NMR spectra of PVIm; (b) ^{1}H-NMR spectra of allyl bromide.

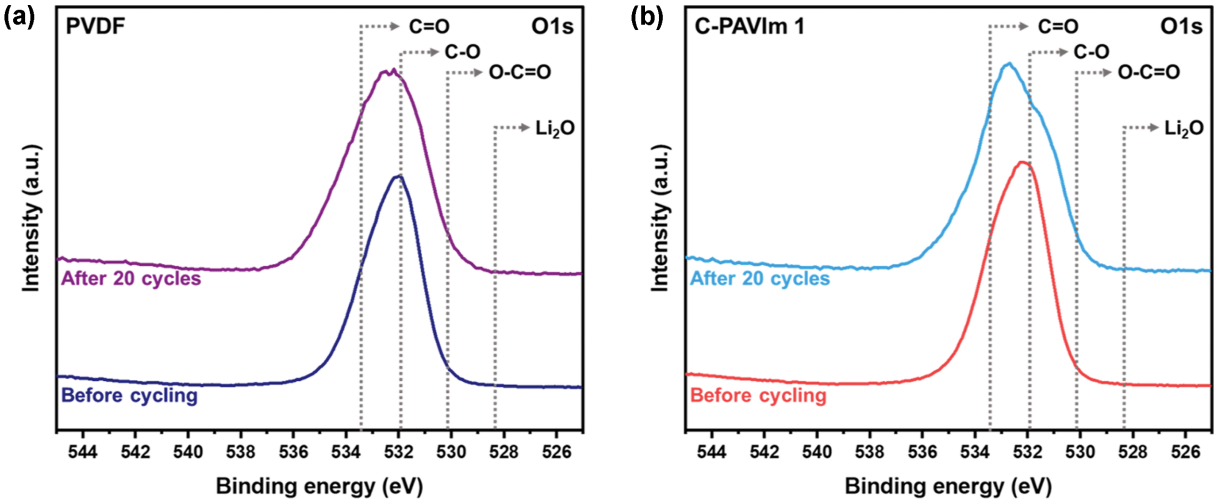

Fig. S3. XPS spectra for before cycling and after 20 cycles: (a) PVDF O1s; (b) C-PAVIm 1 O1s.